THE JOURNAL OF PHYSICAL CHEMISTRY C

Article

pubs.acs.org/JPCC

On the Nature of Defects in Liquid-Phase Exfoliated Graphene

M. V. Bracamonte,*[,†] G. I. Lacconi,[‡] S. E. Urreta,[†] and L. E. F. Foa Torres[†]

[†]Instituto de Física Enrique Gaviola (CONICET) and FaMAF, Universidad Nacional de Córdoba, 5000 Córdoba, Argentina

[‡]INFIQC, Departamento de Fisicoquímica, Facultad de Ciencias Químicas, Universidad Nacional de Córdoba, 5000 Córdoba, Argentina

Supporting Information

ABSTRACT: Liquid-phase exfoliation is one of the most promising routes for large-scale production of multilayer graphene dispersions. These dispersions, which may be used in coatings, composites, or paints, are believed to contain disorder-free graphene multilayers. Here, we address the nature of defects in such samples obtained by liquid-phase exfoliation of graphite powder in *N*-methyl-2-pyrrolidone. Our Raman spectroscopy data challenge the assumption that these multilayers are free of bulk defects, revealing that defect localization strongly depends on the sonication time. For short ultrasound times, defects are located mainly at the layer edges but they turn out to build up in the bulk for ultrasonic times above 2 h. This knowledge may help to devise better strategies to achieve high-quality graphene dispersions.

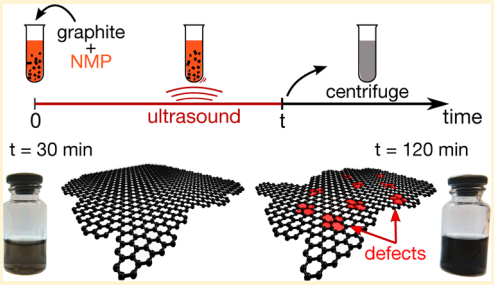

1. INTRODUCTION

Graphene, the ultimate two-dimensional form of carbon, was discovered less than a decade ago.[1−3] Since that seminal discovery, graphene has united many of the electrical,[4] thermal,[5] and mechanical[6] records known to man. Besides allowing the study of puzzling properties predicted for Dirac massless fermions,[4,7] graphene and the related materials also attract an unprecedented attention from technology.[8] Indeed, its versatility allows for a wide range of expected applications, including large displays,[9] optoelectronic devices, and ultracapacitors, and also conductive inks that may allow for ubiquitous printed electronics.[10−12]

Such a broad spectrum of applications requires very different production methods. On one hand, CVD stands as the most viable technique for large-area samples.[9] On the other hand, mass production of micrometer-sized samples for conductive inks requires cost-effective alternatives such as liquid-phase exfoliation of graphite.[13] By immersion of graphite powder in a suitable solvent, it can be exfoliated by using ultrasound (20−100 kHz). The process is simple and effective: ultrasonic waves produce a cavitation process that ultimately leads to the graphite exfoliation, while the solvent prevents the exfoliated multilayers from restacking. The simplicity and relatively low cost of this method have triggered a lot of attention,[11,13−15] and it has been demonstrated to be effective for the production of inkjet printed transistors.[11] Unlike early methods involving oxidation of graphite, followed by liquid exfoliation,[16] here, the π-orbitals are not disrupted, and therefore, the samples are expected to have higher conductivity and a reduced defect density. Concerning this latter technique, however, a few crucial questions remain open: What is the nature of the defects at the origin of the observed defect density evidenced by the D band in the Raman spectra? Does the D band stem only from the edges,[17] or are there bulk defects? Is it possible to control the character of the dominant defects by changing the external parameters?

In this paper, we shed light on some of these questions. We present results for liquid-phase exfoliated graphene multilayers in *N*-methyl-2-pyrrolidone (NMP) obtained after different ultrasonic times and further characterized through Raman spectroscopy, UV−vis spectrophotometry, and scanning electron microscopy (SEM) techniques. From our statistical study of the correlation of the relative intensities of the D and G bands with the width of the latter, we show the existence of a transition between samples with edge-dominated defects and bulk-dominated defects. This transition occurs as the ultrasonic time is increased, indicating that actually shorter ultrasound times may help to obtain high-quality samples. Our analysis of the Raman spectra suggests that the defects are neither vacancies nor sp^3-like defects, leaving the formation of topological defects as a result of the cavitation process as the more likely alternative.

2. EXPERIMENTAL PROCEDURE

Among the many different solvents that could be used to produce the graphene dispersions, such as *N*,*N*-dimethylacetamide (DMA) and *N*,*N*-dimethylformamide (DMF), we chose *N*-methyl-2-pyrrolidone (NMP). NMP is one of the best candidates because of its high boiling point and heat of vaporization, which help in reducing the coffee-ring effect when drying after printing. Besides, NMP also improves the relative

Received: February 24, 2014
Revised: June 6, 2014

   dx.doi.org/10.1021/jp501930a | J. Phys. Chem. C XXXX, XXX, XXX−XXX

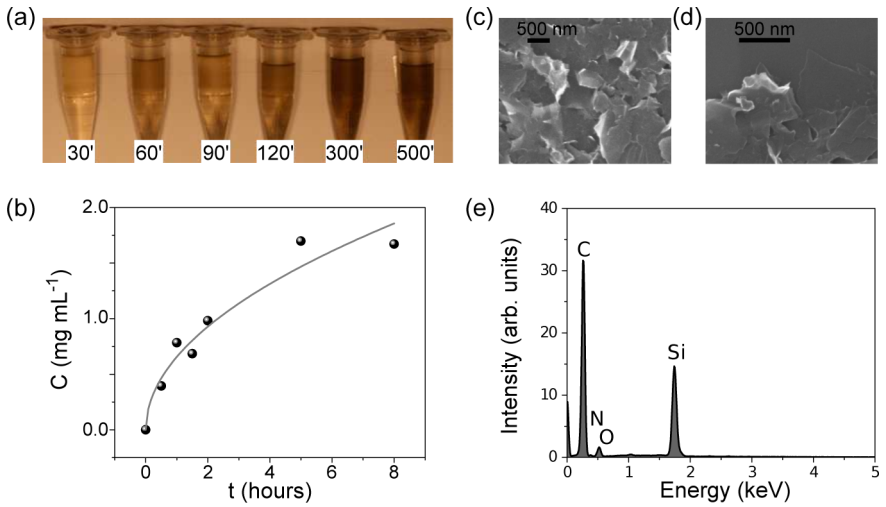

Figure 1. (a) Dispersions of graphene multilayers in NMP. The darker the color, the higher the concentration of the dispersion. (b) Concentration C of dispersed graphene as a function of sonication time t. Dots represent the experimental data and the solid line the best fit obtained with a square root dependence $C = kt^{1/2}$. (c, d) Typical SEM images of flakes deposited on n-doped Si substrate (sonication time of 120 min). (e) EDS spectra for flakes sonicated for t = 300 min confirming the absence of a significative amount of oxides or other contaminants.

stability of the produced dispersions (we checked this in our samples, which remained stable for more than 6 months). Furthermore, it is known that the surface tension of this solvent is similar to that of carbon-based materials (4050 mJ/m^2), thereby allowing graphite exfoliation.

The graphene dispersions reported in this paper were prepared by adding graphite powder (grade #38, Fischer Scientific) to NMP at a concentration of 3.0 mg mL^{-1} and then exposing the dispersions to ultrasound (sonic bath Testlab, TB02, 40 kHz with a power of 80 W). The sonication times ranged between 30 and 500 min, while keeping the water bath temperature below 32 °C. All samples were sonicated at the same spot in the sonic bath. After sonication, the dispersions were centrifuged (centrifuge Arcano, 80-2B) at 500 rpm for 30 min. After centrifugation, the top 80% of the supernatant was collected.

UV−vis absorption spectroscopy was performed with a Shimazdu UV-1700 spectrophotometer using a quartz cuvette with a 1.0 cm optical path. Raman spectra were collected with a LABRAM-HR Horiba Jobin-Yvon confocal microscope at 514 nm and a 100× objective lens with a numerical aperture of 0.9. To avoid sample damage or laser-induced heating, the incident power was kept below 1 mW. The Raman spectra were collected on numerous spots on the sample deposited onto a 300 nm SiO_2/Si wafer. The spectra have been deconvoluted with Lorentzian line shapes for all peaks (these line shapes give the best r^2 = 0.99). The intensity ratio i(D)/i(G) was obtained after a baseline correction. All measurements were performed at room temperature.

Scanning electron microscopy (SEM) images were obtained with a field emission gun scanning electron microscope (FE-SEM, Zeiss, SIGMA model) working at 10 kV.

3. RESULTS AND DISCUSSION

3.1. Effect of Sonication Time on Graphene Concentration. Graphene dispersions with a concentration (graphite powder in NMP) of 3.0 mg mL^{-1} were sonicated during 0.5, 1.0, 2.0, 5.0, and 8.0 h. After centrifugation at 500 rpm, the graphene concentration C was determined from the measured absorbance by using the Lambert−Beer law,[18] $A/l = \alpha C$, with α = 3620 L·g^{-1}·m^{-1} and l the cell length. After dilution, dispersions appeared darker in color at longer sonication times, indicating a higher concentration (see Figure 1a). Figure 1b shows the evolution of the resulting graphene concentration C as a function of the sonication time t.

We find that the data in Figure 1b are well described by the empirical law $C = kt^{1/2}$, where C is the graphene concentration and t is the sonication time (in hours). The constant k is determined by fitting the above expression. The obtained value is k = (0.66 ± 0.03) mg·mL^{-1}·h$^{-1/2}$, suggesting that the concentration is controlled by the flake size, in good agreement with previously reported values.[14,17,18] SEM images show the presence of exfoliated flakes (see Figure 1c,d). The typical lateral dimension determined from STEM measurements is 800 nm. The size distribution spans from 200 nm to 2 μm with 70% of the samples below 1 μm (see also the Supporting Information).

3.2. Raman Characterization. Raman spectroscopy is one of the most useful tools for the characterization of graphene-based materials.[19,20] Here, we take advantage of this powerful nondestructive tool to characterize our samples. After depositing them onto SiO_2/Si wafers, the corresponding Raman spectra were measured at room temperature. Figure 2 shows typical results for different samples corresponding to sonication times of 30, 90, 120, and 300 min. For reference, the spectrum for the pristine graphite powder is also shown at the bottom. The 2D peak (~2709 cm^{-1}) in the spectra of Figure 2 can be identified as the typical signal arising from multilayer graphene.[19,21] The D and G bands were well resolved for all the samples that we measured, appearing at ~1353 and ~1582 cm^{-1}, respectively.

We emphasize that the Raman spectra show no evidence of graphene oxide formation, as expected for the liquid-phase technique used here. This was additionally tested by EDS spectra measurements. Figure 1e shows the spectrum corresponding to a 300 min exfoliated graphene sample where the main carbon signal (74.9 wt %) is observed. Other signals, such as oxygen and nitrogen, associated with the retained solvent or other oxygen containing groups, are hardly

dx.doi.org/10.1021/jp501930a | J. Phys. Chem. C XXXX, XXX, XXX−XXX

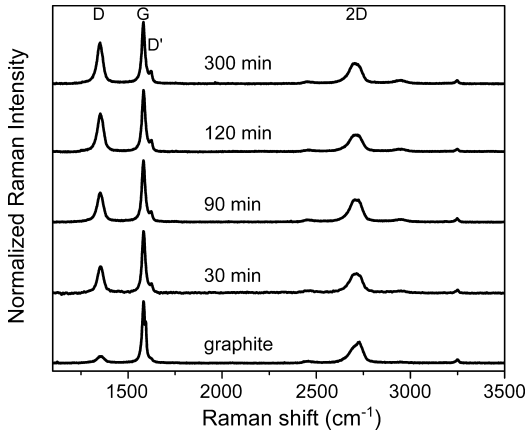

Figure 2. Raman spectra of the graphene samples obtained for different sonication times (30, 90, 120, and 300 min). The spectrum of a pristine graphite sample is also shown for reference (bottom). All the samples were centrifuged at 500 rpm for 30 min. The spectra show four main signals: D at ∼1353 cm^{-1}, G at ∼1582 cm^{-1}, D′ at ∼1622 cm^{-1}, and the 2D band at ∼2709 cm^{-1}. Furthermore, a few combinations of them are also observed: D + D″ at ∼2450 cm^{-1}, D + D′ at ∼2952 cm^{-1}, and G* at ∼3246 cm^{-1}.

detected, whereas the Si peaks certainly arise from the substrate.

Defects in the graphene structure break symmetries,[7,22] thereby allowing otherwise forbidden inter/intravalley processes that lead to the D and D′ bands. These defects can be either the sample edges[23,24] or the bulk defects,[19] and a very important question is whether one could distinguish and quantify different defects based on the Raman spectra.[19,23−26]

The quantity of defects has been shown to be related to the ratio between the D and G bands, $i(D)/i(G)$; the larger the ratio, the larger the defect density (and, therefore, the typical distance between defects).[25,26] As we will see below, we observe that $i(D)/i(G)$ increases with increasing the sonication time, thereby indicating an increase in the defect density. The typical distance between defects can be estimated to be in the range between 10 and 20 nm. In the following, we focus on a more subtle point concerning the type and location of the emerging defects.

We would like to establish whether or not the D and D′ signals mainly stem from sample edges and whether this holds for all sonication times t. Inspection of the individual Raman signals or of average peak positions/widths for the different values of t did not show any clear trend. Therefore, we decided to check for correlations between the amount of disorder as quantified by $i(D)/i(G)$ and the full width at half-maximum (FWHM) of the G band. As we comment below, this correlation provides valuable information on the origin of the D band. The results are shown in Figure 3 for t = 30 min (a), t = 90 min (b), t = 120 min (c), and t = 300 min (d). Whereas, for short sonication times, the data show no statistical correlation between $i(D)/i(G)$ and FWHM(G), this changes dramatically in panels (c) and (d) (t = 120, 300 min): as the sonication time increases, confidence bands (dashed lines) stretch closer to the best fit and one can see that larger $i(D)/i(G)$ values are correlated with larger widths of the G band.

To rationalize the origin and meaning of the observed correlation between $i(D)/i(G)$ and the width of the G band, we argue on a few key facts. The first one is that a larger $i(D)/i(G)$ ratio indicates a larger amount of either bulk disorder[25,26] or

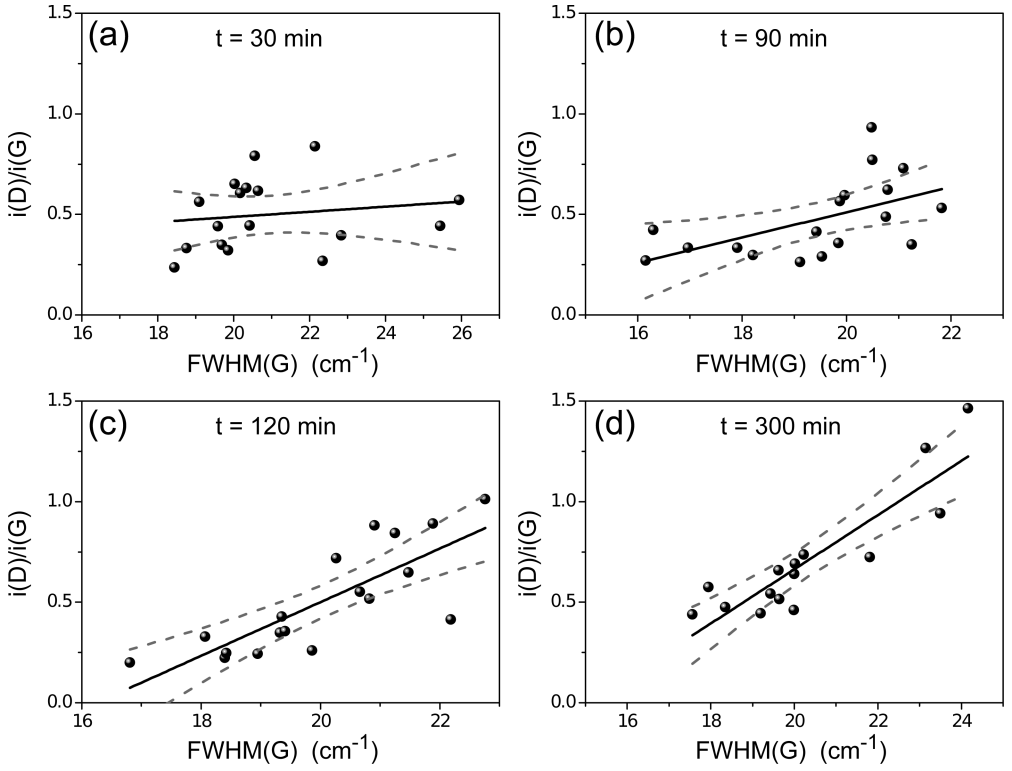

Figure 3. $i(D)/i(G)$ versus FWHM(G) plots for dispersions sonicated for 30 (a), 90 (b), 120 (c), and 300 (d) min. The dots are experimental data. To ensure homogeneity in the conditions, the data in each plot correspond to flakes from the same dispersion. The solid lines are a linear fit to the data; 95% confidence bands are also indicated with dashed lines.

dx.doi.org/10.1021/jp501930a | J. Phys. Chem. C XXXX, XXX, XXX−XXX

edges,[27] but it cannot discriminate between them. On the other hand, it turns out that the width of the G band (FWHM(G)) increases with bulk disorder (see, for example, Figure 5 of ref 26, where FWHM(G) is shown to increase when the interdefect distance decreases), but it does not increase when introducing edges.[30] Therefore, samples with a larger amount of bulk disorder (exhibiting a larger $i(D)/i(G)$) should also have a larger FWHM(G); i.e., $i(D)/i(G)$ should be positively correlated with FWHM(G). In contrast, samples with no bulk disorder should show no correlation between the two magnitudes, as reported in ref 11.

These two facts allow us to conclude that the transition observed in our data is likely to be produced by an increase in *bulk disorder* when passing from t = 30 min to t = 120 min. These trends are also found if the area of the D and G peaks ($A(D)$ and $A(G)$) are considered; i.e., $A(D)/A(G)$ directly correlates with FWHM(G). This is shown in Figure S2 of the Supporting Information.

To further confirm the above conclusions, we devised a simple additional experiment. If bulk disorder is created for longer sonication times, then annealing the samples should restore a low correlation between $i(D)/i(G)$ versus FWHM(G). Figure 4 shows the results for samples sonicated for 120 min before and after annealing at 600 °C for 1 h in high vacuum. The data reveal a reduction in the $i(D)/i(G)$ values after annealing, indicating a lower disorder comparable with the values achieved with shorter sonication times (30 and 90 min in Figure 3a, b). Whether this smaller $i(D)/i(G)$ ratio is mainly due to bulk defects or not can be inferred from the correlation between $i(D)/i(G)$ and FWHM(G); Figure 4 shows no correlation between these magnitudes, which, as argued before, can only be explained by edges rather than bulk defects. This indicates that most of the bulk defects have been repaired by the annealing process. In contrast, the same thermal treatment applied to flakes sonicated for 30 min does not appreciably change the slope of the relation observed in Figure 3a (see the Supporting Information, Figure S3). In summary, our observations in Figures 3 and 4 indicate a transition from samples with an edge-dominated D band to more disordered structures where bulk defects dominate, the latter emerging when the sonication time is increased.

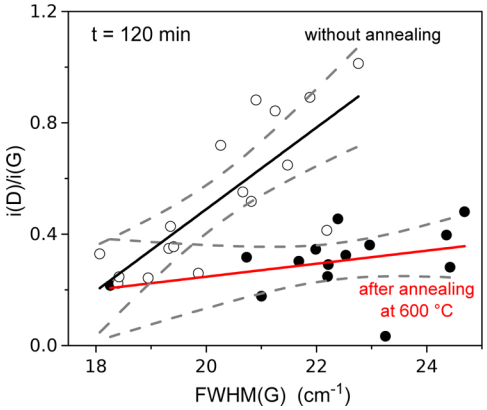

Figure 4. $i(D)/i(G)$ as a function of FWHM(G) for a dispersion sonicated for 120 min. Empty circles correspond to the samples before annealing, while full black circles are for the samples after annealing at 600 °C. The solid line indicates the best linear fit to the data; 95% confidence bands are also indicated in the figure with dashed lines.

Up to now, we have presented evidence that, in our liquid-phase exfoliated samples, bulk defects (in contrast to edges) become dominant (as evidenced in the Raman D band) when the sonication time is about 120 min. A natural question then concerns the specific type of defects produced at this transition. Here, we give some possible directions supported by our data. The possible defects include topological defects (like pentagon−heptagon pairs), vacancies, substitutional impurities, and sp^3-like defects.[7] Recent studies show that the ratio between the D and D′ lines is very sensitive to the type of defect,[28] with studies reporting a ratio of 3.5 for boundaries, 7 for vacancies, 13 for sp^3, and values in-between those for vacancies and sp^3 for substitutional impurities.[23,24] The fact that, for all sonication times, our samples show a roughly constant $i(D)/i(D')$ ratio of (4.5 ± 0.5) rules out vacancies, substitutions, and sp^3 defects. Moreover, since topological defects have the lowest formation energy,[29] we conclude that this is the most likely defect that emerges as the sonication time is increased. In this sense, different results when using a bath sonicator as in our work or a tip sonicator, as reported in ref 11, cannot be ruled out.[31] In any case, lower ultrasound power may help in getting better samples.

On the basis of the conclusions of the previous paragraph, ruling out sp^3 or substitutional impurities, a possible mechanism for the creation of bulk defects could be attributed to the cavitation process. Increasing the sonication time would then increase the probability of defect formation and, therefore, the defect density. Numerical simulations may shed light on this issue.

4. FINAL REMARKS

We present a statistical study of the Raman spectra of graphene multilayers dispersed in NMP by liquid-phase exfoliation. Our results reveal the building up of bulk disorder as the sonication time increases. This is reflected in the evolution of the correlation between the ratio of the D to G band intensities ($i(D)/i(G)$) and the width of the G band. Our results suggest that low disorder samples require a careful tuning of the ultrasonic times. Otherwise, sample annealing may largely enhance the sample's crystalline quality, leading to a better material for applications such as composites and conductive inks.

Further analysis of the obtained Raman spectra suggests that the bulk defects are not vacancies, nor substitutional impurities or sp^3-like, but rather topological defects. The precise mechanism leading to defect formation, which is likely to result from the cavitation process, remains as an interesting subject of study.

■ ASSOCIATED CONTENT

Supporting Information

The lateral size distribution of our samples as determined by STEM is included in the Supporting Information. $A(D)/A(G)$ versus FWHM(G) is shown in Figure S2. The annealing experiment for the samples sonicated during 30 min is shown in Figure S3. This material is available free of charge via the Internet at http://pubs.acs.org.

■ AUTHOR INFORMATION

Corresponding Author

*Phone: 54 351 4334051. E-mail: vbracamonte@famaf.unc.edu.ar.

dx.doi.org/10.1021/jp501930a | J. Phys. Chem. C XXXX, XXX, XXX−XXX

Notes

The authors declare no competing financial interest.

■ ACKNOWLEDGMENTS

We acknowledge financial support from ANPCyT Project PICT PRH 61 and SeCyT-UNC. L.E.F.F.T. acknowledges the support of Trieste's ICTP. M.V.B. thanks CONICET for the fellowship. M.V.B. thanks Dr. Arlene O'Neill for useful technical comments. G.I.L. acknowledges projects PICT-324 and PME (2006) 1544. We thank Dr. Paula Bercoff for taking the SEM images presented here as well as Dr. Luis Fabietti for technical help.

■ REFERENCES

(1) Novoselov, K. S.; Geim, A. K.; Morozov, S. V.; Jiang, D.; Zhang, Y.; Dubonos, S. V.; Grigorieva, I. V.; Firsov, A. A. Electric Field Effect in Atomically Thin Carbon Films. *Science* **2004**, *306*, 666−669.

(2) Novoselov, K. S.; Geim, A. K.; Morozov, S. V.; Jiang, D.; Katsnelson, M. I.; Grigorieva, I. V.; Dubonos, S. V.; Firsov, A. A. Two-Dimensional Gas of Massless Dirac Fermions in Graphene. *Nature* **2005**, *438*, 197−200.

(3) Zhang, Y.; Tan, Y.-W.; Stormer, H. L.; Kim, P. Experimental Observation of the Quantum Hall Effect and Berry's Phase in Graphene. *Nature* **2005**, *438*, 201−204.

(4) Geim, A. K.; Novoselov, K. S. The Rise of Graphene. *Nat. Mater.* **2007**, *6*, 183−191.

(5) Balandin, A. A.; Ghosh, S.; Bao, W.; Calizo, I.; Teweldebrhan, D.; Miao, F.; Lau, C. N. Superior Thermal Conductivity of Single-Layer Graphene. *Nano Lett.* **2008**, *8*, 902−907.

(6) Lee, C.; Wei, X.; Kysar, J. W.; Hone, J. Measurement of the Elastic Properties and Intrinsic Strength of Monolayer Graphene. *Science* **2008**, *321*, 385−388.

(7) Foa Torres, L. E. F.; Roche, S.; Charlier, J. C. *Introduction to Graphene-Based Nanomaterials: From Electronic Structure to Quantum Transport*; Cambridge University Press: Cambridge, U.K., 2014.

(8) Novoselov, K. S.; Falko, V. I.; Colombo, L.; Gellert, P. R.; Schwab, M. G.; Kim, K. A Roadmap for Graphene. *Nature* **2012**, *490*, 192−200.

(9) Bae, S.; Kim, H.; Lee, Y.; Xu, X.; Park, J.-S.; Zheng, Y.; Balakrishnan, J.; Lei, T.; Kim, H. R.; Song, Y. I.; et al. Roll-to-Roll Production of 30-in. Graphene Films for Transparent Electrodes. *Nat. Nanotechnol.* **2010**, *5*, 574−578.

(10) Emtsev, K. V.; Bostwick, A.; Horn, K.; Jobst, J.; Kellogg, G. L.; Ley, L.; McChesney, J. L.; Ohta, T.; Reshanov, S. A.; Rohrl, J.; et al. Towards Wafer-Size Graphene Layers by Atmospheric Pressure Graphitization of Silicon Carbide. *Nat. Mater.* **2009**, *8*, 203−207.

(11) Torrisi, F.; Hasan, T.; Wu, W.; Sun, Z.; Lombardo, A.; Kulmala, T. S.; Hsieh, G.-W.; Jung, S.; Bonaccorso, F.; Paul, P. J.; et al. Inkjet-Printed Graphene Electronics. *ACS Nano* **2012**, *6*, 2992−3006.

(12) Han, X.; Chen, Y.; Zhu, H.; Preston, C.; Wan, J.; Fang, Z.; Hu, L. Scalable, Printable, Surfactant-Free Graphene Ink Directly from Graphite. *Nanotechnology* **2013**, *24*, 205304.

(13) Nicolosi, V.; Chhowalla, M.; Kanatzidis, M. G.; Strano, M. S.; Coleman, J. N. Liquid Exfoliation of Layered Materials. *Science* **2013**, DOI: 10.1126/science.1226419.

(14) Khan, U.; Porwal, H.; O Neill, A.; Nawaz, K.; May, P.; Coleman, J. N. Solvent-Exfoliated Graphene at Extremely High Concentration. *Langmuir* **2011**, *27*, 9077−9082.

(15) Paton, K. R.; Varrla, E.; Backes, C.; Smith, R. J.; Khan, U.; O'Neill, A.; Boland, C.; Lotya, M.; Istrate, O. M.; King, P.; et al. Scalable Production of Large Quantities of Defect-Free Few-Layer Graphene by Shear Exfoliation in Liquids. *Nat. Mater.* **2014**, *13*, 624−630.

(16) Stankovich, S.; Dikin, D. A.; Dommett, G. H. B.; Kohlhaas, K. M.; Zimney, E. J.; Stach, E. A.; Piner, R. D.; Nguyen, S. T.; Ruoff, R. S. Graphene-Based Composite Materials. *Nature* **2006**, *442*, 282−286.

(17) Khan, U.; O'Neill, A.; Lotya, M.; De, S.; Coleman, J. N. High-Concentration Solvent Exfoliation of Graphene. *Small* **2010**, *6*, 864−871.

(18) Coleman, J. N. Liquid Exfoliation of Defect-Free Graphene. *Acc. Chem. Res.* **2013**, *46*, 14−22.

(19) Ferrari, A. C.; Basko, D. M. Raman Spectroscopy as a Versatile Tool for Studying the Properties of Graphene. *Nat. Nanotechnol.* **2013**, *8*, 235−246.

(20) Jorio, A.; Dresselhaus, M.; Saito, R.; Dresselhaus, G. F. *Raman Spectroscopy in Graphene Related Systems*; Wiley-VCH: Weinheim, Germany, 2011.

(21) Cong, C.; Yu, T.; Saito, R.; Dresselhaus, G. F.; Dresselhaus, M. S. Second-Order Overtone and Combination Raman Modes of Graphene Layers in the Range of 1690−2150 cm^{-1}. *ACS Nano* **2011**, *5*, 1600−1605.

(22) Terrones, M.; Botello-Méndez, A. R.; Campos-Delgado, J.; López-Urías, F.; Vega-Cantú, Y. I.; Rodríguez-Macías, F. J.; Elas, A. L.; Muñoz Sandoval, E.; Cano-Marquez, A. G.; Charlier, J.-C.; et al. Graphene and Graphite Nanoribbons: Morphology, Properties, Synthesis, Defects and Applications. *Nano Today* **2010**, *5*, 351−372.

(23) Eckmann, A.; Felten, A.; Mishchenko, A.; Britnell, L.; Krupke, R.; Novoselov, K. S.; Casiraghi, C. Probing the Nature of Defects in Graphene by Raman Spectroscopy. *Nano Lett.* **2012**, *12*, 3925−3930.

(24) Eckmann, A.; Felten, A.; Verzhbitskiy, I.; Davey, R.; Casiraghi, C. Raman Study on Defective Graphene: Effect of the Excitation Energy, Type, and Amount of Defects. *Phys. Rev. B* **2013**, *88*, 035426.

(25) Ferrari, A. C.; Robertson, J. Interpretation of Raman Spectra of Disordered and Amorphous Carbon. *Phys. Rev. B* **2000**, *61*, 14095−14107.

(26) Cancado, L. G.; Jorio, A.; Ferreira, E. H. M.; Stavale, F.; Achete, C. A.; Capaz, R. B.; Moutinho, M. V. O.; Lombardo, A.; Kulmala, T. S.; Ferrari, A. C. Quantifying Defects in Graphene via Raman Spectroscopy at Different Excitation Energies. *Nano Lett.* **2011**, *11*, 3190−3196.

(27) Cancado, L. G.; Pimenta, M. A.; Neves, B. R. A.; Dantas, M. S. S.; Jorio, A. Influence of the Atomic Structure on the Raman Spectra of Graphite Edges. *Phys. Rev. Lett.* **2004**, *93*, 247401.

(28) Venezuela, P.; Lazzeri, M.; Mauri, F. Theory of Double-Resonant Raman Spectra in Graphene: Intensity and Line Shape of Defect-Induced and Two-Phonon Bands. *Phys. Rev. B* **2011**, *84*, 035433.

(29) Li, L.; Reich, S.; Robertson, J. Defect Energies of Graphite: Density-Functional Calculations. *Phys. Rev. B* **2005**, *72*, 184109.

(30) Casiraghi, C.; Hartschuh, A.; Qian, H.; Piscanec, C.; Georgi, C.; Fasoli, A.; Novoselov, K. S.; Basko, D. M.; Ferrari, A. C. Raman Spectroscopy of Graphene Edges. *Nano Lett.* **2009**, *9*, 1433−1441.

(31) Buzaglo, M.; Shtein, M.; Kober, S.; Lovrincic, R.; Vilan, A.; Regev, O. Critical Parameters in Exfoliating Graphite into Graphene. *Phys. Chem. Chem. Phys.* **2013**, *15*, 4428−4435.